Australian Government | ANSTO | Queen's University | University of California, Davis | Argonne National Laboratory

On the Measurement of Dislocations and Dislocation Structures using EBSD and HRSD Techniques

O. Muránsky, L. Balogh, M. Tran, C.J. Hamelin, J.-S. Park, M. R. Daymond

Only thanks to the support of many people this paper has happened. Special thank you to T. Palmer (ANSTO), T. Nicholls (ANSTO), Z. Zhang (ANSTO), L. Edwards (ANSTO), and M.R. Hill (UC). I hope you find the paper useful.
/OM

Acta Materialia 175 (2019) 297–313

Contents lists available at ScienceDirect

Acta Materialia

journal homepage: www.elsevier.com/locate/actamat

Full length article

On the measurement of dislocations and dislocation substructures using EBSD and HRSD techniques

O. Muránsky[a,b,*], L. Balogh[c], M. Tran[d,a], C.J. Hamelin[e,a], J.-S. Park[f], M.R. Daymond[c]

[a] Australian Nuclear Science and Technology Organisation, Lucas Heights, NSW, Australia
[b] School of Mechanical and Manufacturing Engineering, UNSW Sydney, Sydney, Australia
[c] Queen's University, Mechanical and Materials Engineering, Kingston, ON, Canada
[d] University of California, Mechanical and Aerospace Engineering, Davis, CA, USA
[e] EDF Energy, Barnwood, Gloucestershire, UK
[f] Advanced Photon Source, Argonne National Laboratory, Lemont, IL, USA

ARTICLE INFO

Article history:
Received 26 March 2019
Received in revised form 14 May 2019
Accepted 17 May 2019
Available online 7 June 2019

Keywords:
Dislocation density
Metal plasticity
Electron back-scatter diffraction (EBSD)
High-resolution synchrotron diffraction (HRSD)
Peak broadening

ABSTRACT

The accumulation of the dislocations and development of dislocation structures in plastically deformed Ni201 is examined using dedicated analyses of Electron Back-Scatter Diffraction (EBSD) acquired orientation maps, and High-Resolution Synchrotron Diffraction (HRSD) acquired patterns. The results show that the minimum detectable microstructure-averaged (bulk) total dislocation density (ρ_T) measured via HRSD is approximately 1E13 m^{-2}, while the minimum GND density (ρ_G) measured via EBSD is approximately 2E12 m^{-2} – the EBSD technique being more sensitive at low plastic strain. This highlights complementarity of the two techniques when attempting to quantify amount of plastic deformation (damage) in a material via a measurement of present dislocations and their structures. Furthermore, a relationship between EBSD-measured ρ_G and the size of HRSD-measured Coherently Scattering Domains (CSDs) has been mathematically derived – this allows for an estimation of the size of CSDs from EBSD-acquired orientation maps, and conversely an estimation of ρ_G from HRSD-measured size of CSDs. The measured evolution of ρ_T, and ρ_G is compared with plasticity theory models – the current results suggest that Ashby's single-slip model underestimates the amount of GNDs (ρ_G), while Taylor's model is correctly predicting the total amount of dislocation (ρ_T) present in the material as a function of imparted plastic strain.

ondrej.muransky@ansto.gov.au

Dislocations & Sub-Grain Structure

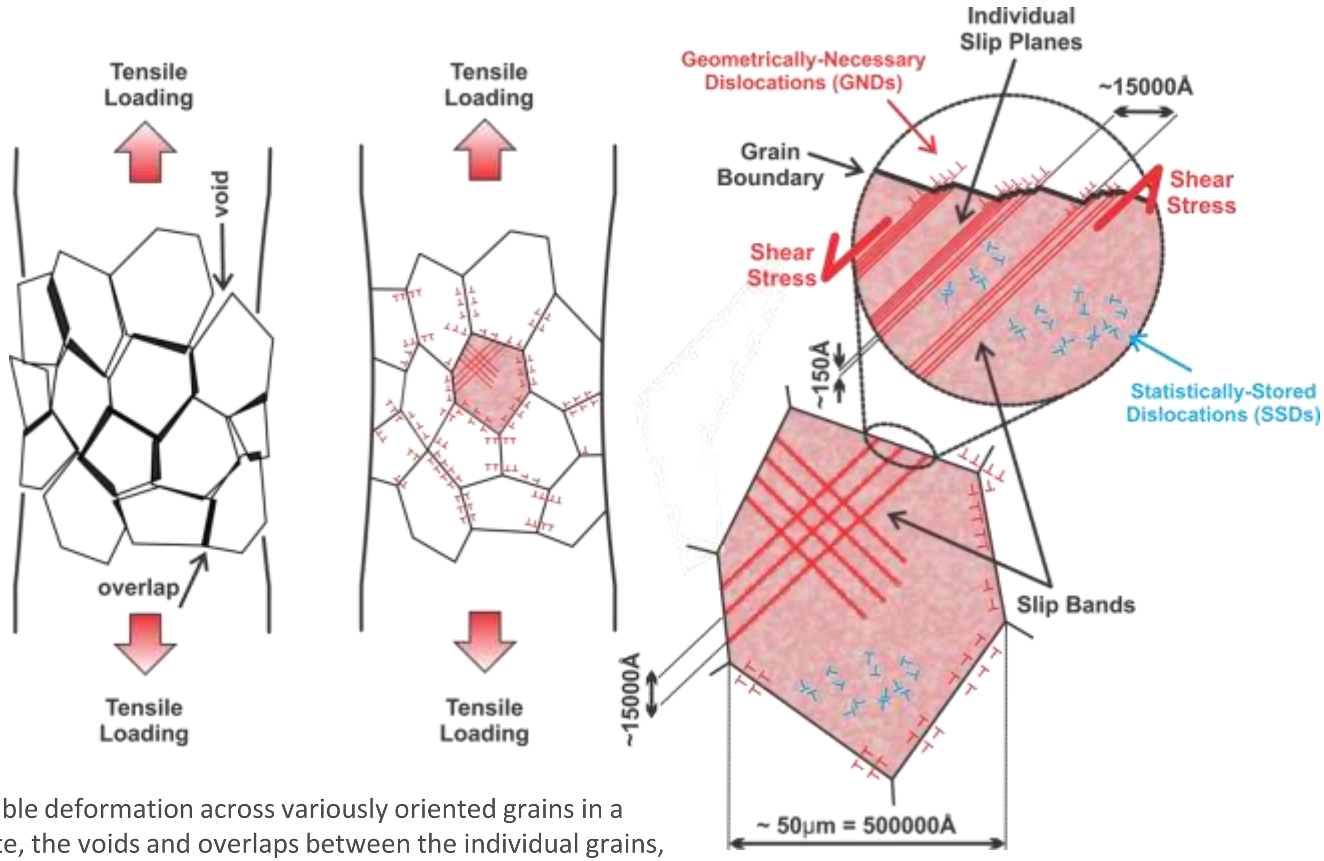

⇒ To maintain compatible deformation across variously oriented grains in a polycrystalline aggregate, the voids and overlaps between the individual grains, which would otherwise appear due to the crystallites (grains) anisotropy are corrected by the storing a portion of dislocations in the form of geometrically-necessary dislocations (GNDs). Plastically deformed material also stores so-called statistically-stored dislocations (SSDs), which are stored by mutual random trapping. Both GNDs and SSDs arrange themselves into energetically favourable configurations, forming geometrically-necessary boundaries (GNBs) and incidental dislocation boundaries (IDBs), respectively.

Experiment

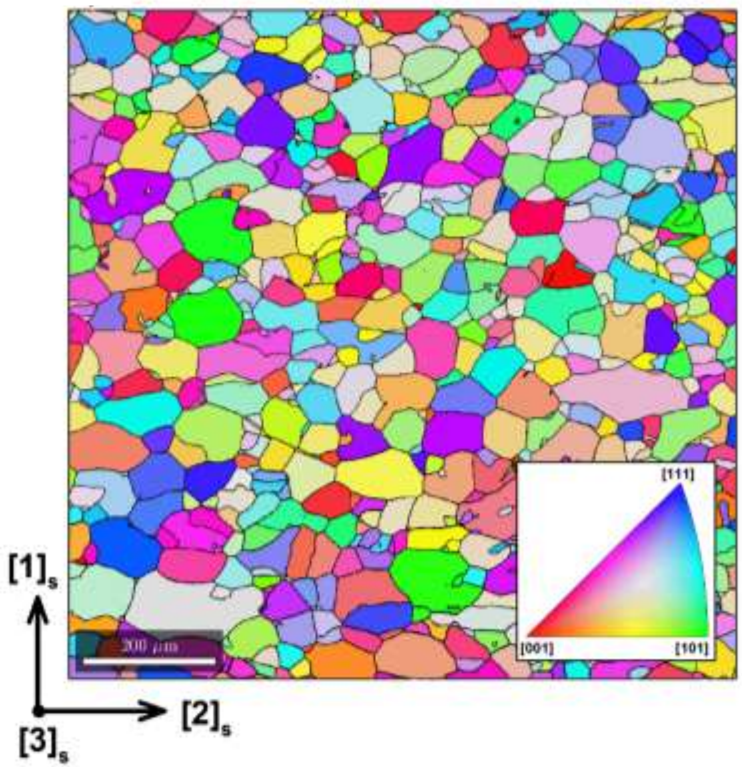

⇒ EBSD orientation map showing the overall equiaxed grain structure of our solution-annealed Ni201 before testing.

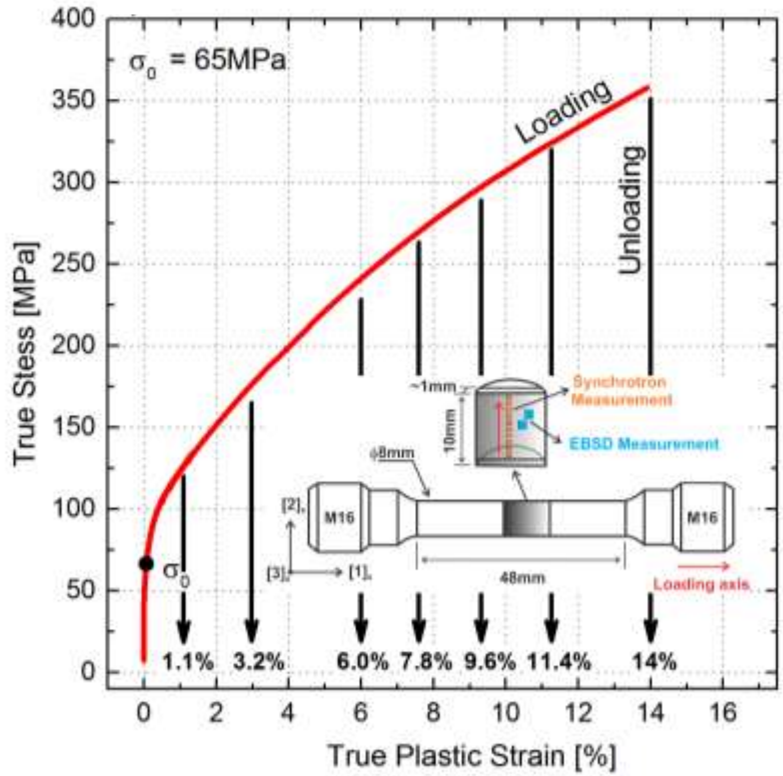

⇒ Interrupted tensile tests were performed to varying levels of imparted plastic strain. Samples were extracted from the gauge length for EBSD and HRSD measurement.

Ni-201

Ni	C	Si	P	Fe	Mn	Cr	Mo	Cu	V	Nb	Ti	Al
bal.	<0.01	0.07	<0.01	0.03	<0.01	<0.01	<0.01	0.01	<0.01	<0.01	0.07	<0.01

ANSTO

EBSD Measurements

Electron Back-Scatter Diffraction (EBSD)

⇒ EBSD, is a scanning electron microscope (SEM) based technique that gives crystallographic information about the microstructure of a sample.

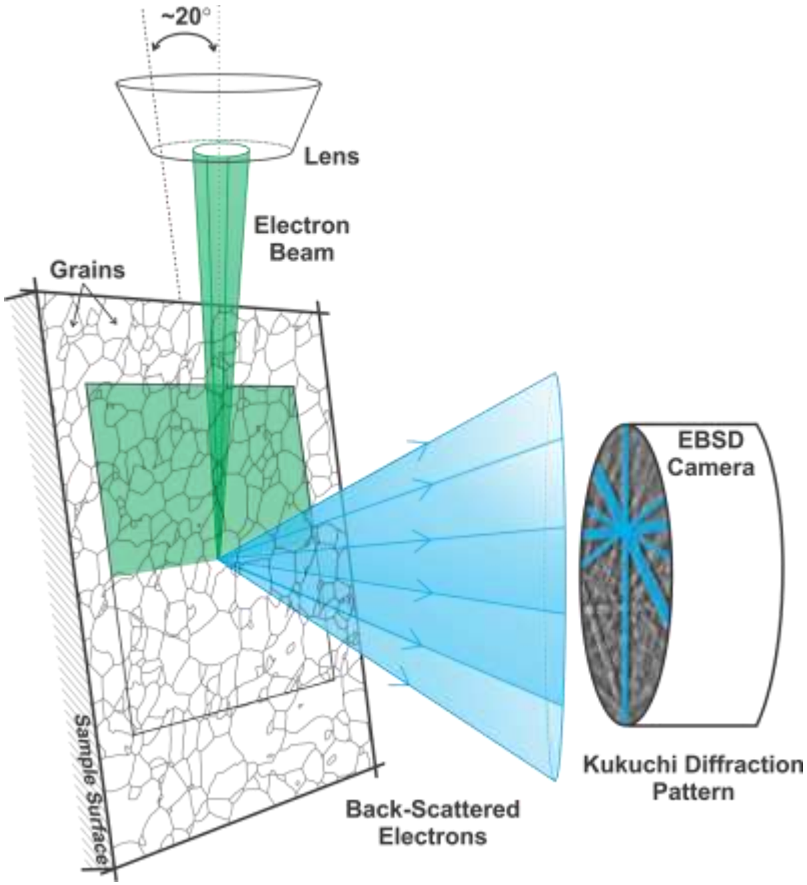

⇒ The data collected with EBSD is spatially distributed and is visualised in so-called EBSD orientation maps.

EBSD & Dislocations

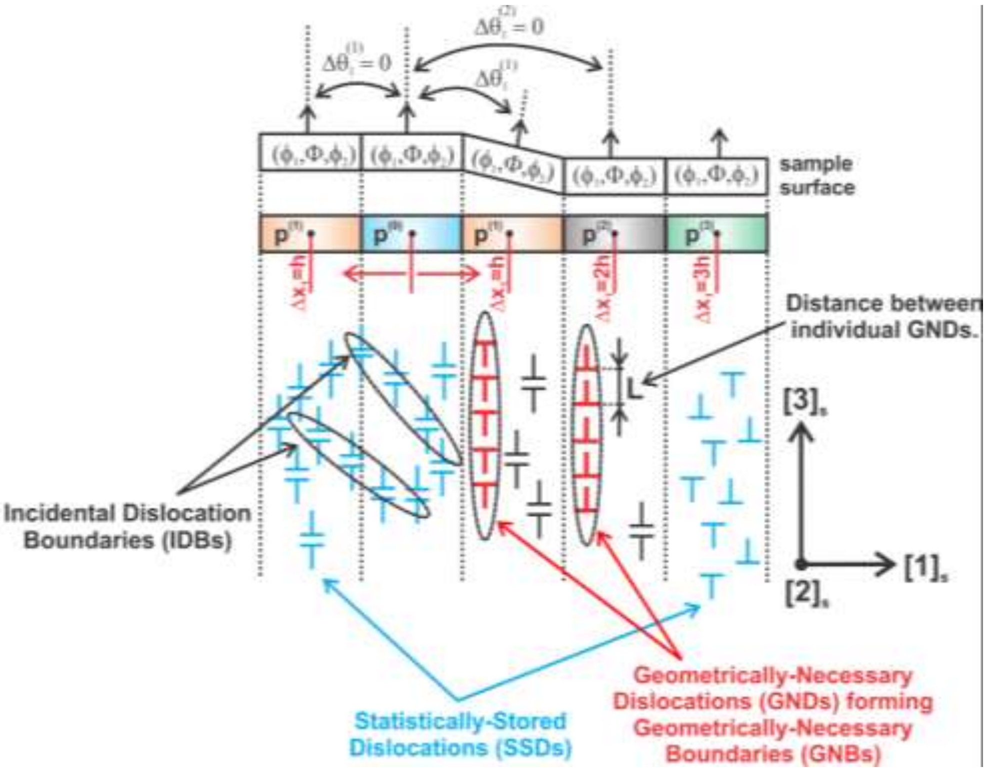

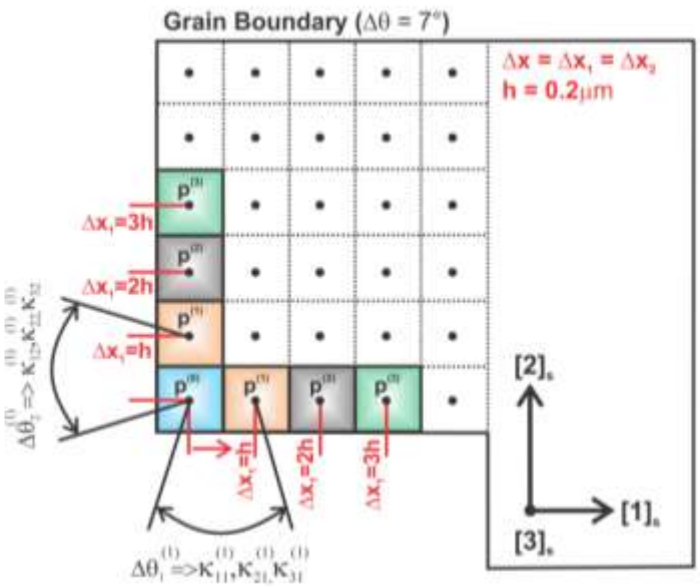

⇒ GNDs have a geometrical consequence giving rise to a curvature of the crystal lattice, which can be measured by EBSD technique. The crystal orientation (ϕ_1,Φ,ϕ_2) changes only when the electron beam crosses an array of GNDs that has a net non-zero Burger's vector.

Lattice Curvature

Misorientation Angle

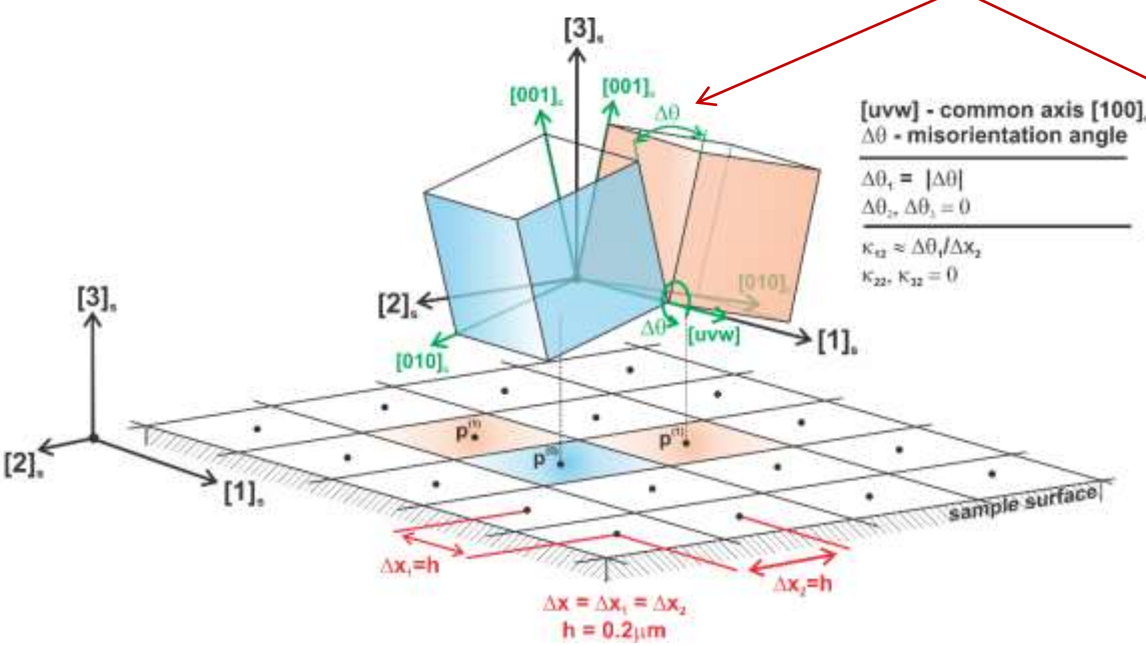

⇒ A schematic representation of lattice curvature components calculation between two neighbouring crystals misoriented ($\Delta\theta$) by a rotation around the common crystallographic axis $[100]_c$ ($[uvw]_c$) and separated by pixel separation distance (Δx_2). Note, that in this example: $\kappa_{12} \approx \Delta\theta_1/\Delta x_2$, and $\kappa_{22}, \kappa_{32} = 0$.

Lattice Curvature Tensor

$$\kappa_{ij} = \begin{bmatrix} \kappa_{11} & \kappa_{12} & \kappa_{13} \\ \kappa_{21} & \kappa_{22} & \kappa_{23} \\ \kappa_{31} & \kappa_{32} & \kappa_{33} \end{bmatrix}$$

$$\kappa_{ij} = \frac{\partial\theta_i}{\partial x_j} \approx \frac{\Delta\theta_i}{\Delta x_j}$$

pixel separation distance, $\Delta \mathbf{x}$

Lattice Curvature Tensor Components

$$\kappa_{11} \approx \frac{\Delta\theta_1}{\Delta x_1}; \kappa_{21} \approx \frac{\Delta\theta_2}{\Delta x_1}; \kappa_{31} \approx \cancel{\frac{\Delta\theta_3}{\Delta x_1}}$$

$$\kappa_{12} \approx \frac{\Delta\theta_1}{\Delta x_2}; \kappa_{22} \approx \frac{\Delta\theta_2}{\Delta x_2}; \kappa_{32} \approx \cancel{\frac{\Delta\theta_3}{\Delta x_2}}$$

ANSTO

Lattice Curvature & GND Density

Line Vector

GND Density

$$\kappa_{ij} = \sum_{t=1}^{N} \left(b_j^t l_i^t - \frac{1}{2} \delta_{ij} b_m^t l_m^t \right) \rho_G^t$$

N = 1 .. 36 – number of possible dislocation types

Burgers Vector

Edge Dislocations: 12
Screw Dislocations: 6

Dislocation Types: 2 x 18 = 36

dislocations of opposite sign needs to be distinguished

1,947,792 possibilities!

$$\begin{bmatrix} \kappa_{11} \\ \kappa_{21} \\ \kappa_{31} \\ \kappa_{12} \\ \kappa_{22} \\ \kappa_{32} \end{bmatrix} = \begin{bmatrix} \frac{1}{2} b_1^1 l_1^1 & \frac{1}{2} b_1^2 l_1^2 & \cdots & \frac{1}{2} b_1^{36} l_1^{36} \\ b_1^1 l_2^1 & b_1^2 l_2^2 & \cdots & b_1^{36} l_2^{36} \\ b_1^1 l_3^1 & b_1^2 l_3^2 & \cdots & b_1^{36} l_3^{36} \\ b_2^1 l_1^1 & b_2^2 l_1^2 & \cdots & b_2^{36} l_1^{36} \\ \frac{1}{2} b_2^1 l_2^1 & \frac{1}{2} b_2^2 l_2^2 & \cdots & \frac{1}{2} b_2^{36} l_2^{36} \\ b_2^1 l_3^1 & b_2^2 l_3^2 & \cdots & b_2^{36} l_3^{36} \end{bmatrix} \begin{bmatrix} \rho_G^1 \\ \rho_G^2 \\ \vdots \\ \vdots \\ \vdots \\ \rho_G^{36} \end{bmatrix}$$

6 known lattice curvatures (measured)

36 possible dislocation types

Lattice Curvature Tensor (κ_{ij})

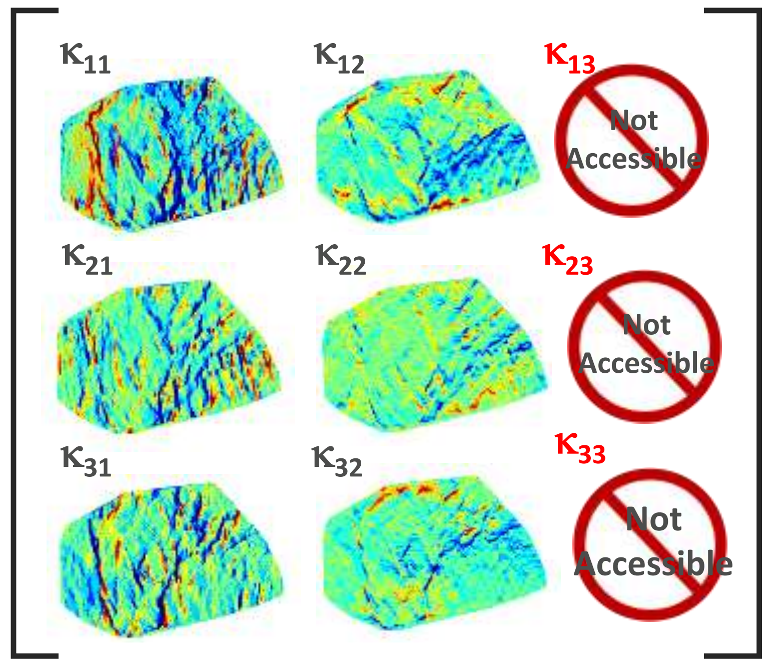

Dislocation Types (fcc)

12× Deformation Modes

$(111)\langle 0\bar{1}1\rangle$

$(\bar{1}11)\langle 0\bar{1}1\rangle$

$(\bar{1}11)\langle 101\rangle$

$(\bar{1}\bar{1}1)\langle 101\rangle$

$(1\bar{1}1)\langle 011\rangle$

$(111)\langle 011\rangle$

$(1\bar{1}1)\langle \bar{1}01\rangle$

$(\bar{1}11)\langle \bar{1}01\rangle$

$(1\bar{1}1)\langle 110\rangle$

$(111)\langle 110\rangle$

$(\bar{1}\bar{1}1)\langle 0\bar{1}0\rangle$

$(\bar{1}\bar{1}1)\langle 0\bar{1}0\rangle$

6× Burger's Vectors

$\vec{b}_1 = \langle 0\bar{1}1\rangle a/2$

$\vec{b}_2 = \langle 101\rangle a/2$

$\vec{b}_3 = \langle 011\rangle a/2$

$\vec{b}_4 = \langle \bar{1}01\rangle a/2$

$\vec{b}_5 = \langle 110\rangle a/2$

$\vec{b}_6 = \langle 0\bar{1}0\rangle a/2$

12× Line Vectors

$\vec{b} \perp \vec{t}$

$\vec{t}_1 = \vec{b}_1 \times \vec{n}_1$

$\vec{t}_2 = \vec{b}_1 \times \vec{n}_2$

$\vec{t}_3 = \vec{b}_2 \times \vec{n}_3$

$\vec{t}_4 = \vec{b}_2 \times \vec{n}_4$

$\vec{t}_5 = \vec{b}_3 \times \vec{n}_5$

$\vec{t}_6 = \vec{b}_3 \times \vec{n}_6$

$\vec{t}_7 = \vec{b}_4 \times \vec{n}_7$

$\vec{t}_8 = \vec{b}_4 \times \vec{n}_8$

$\vec{t}_9 = \vec{b}_5 \times \vec{n}_9$

$\vec{t}_{10} = \vec{b}_5 \times \vec{n}_{10}$

$\vec{t}_{11} = \vec{b}_6 \times \vec{n}_{11}$

$\vec{t}_{12} = \vec{b}_6 \times \vec{n}_{12}$

6× Line Vectors

$\vec{b} \parallel \vec{t}$

$\vec{t}_{13} = \vec{b}_1$

$\vec{t}_{14} = \vec{b}_2$

$\vec{t}_{15} = \vec{b}_3$

$\vec{t}_{16} = \vec{b}_4$

$\vec{t}_{17} = \vec{b}_5$

$\vec{t}_{18} = \vec{b}_6$

Number of Dislocation Types

Edge = 12

Screw = 6

---

18 × 2 = 36

dislocations of opposite sign needs to be distinguished

A. Arsenlis, Acta Matterialia, 47, 1999, pp. 1597-1611.

Lower-Bound GND Density

Line Vector

GND Density

$$\kappa_{ij} = \sum_{t=1}^{N} \left(b_j^t l_i^t - \frac{1}{2}\delta_{ij} b_m^t l_m^t \right) \rho_G^t$$

N = 1 .. 36 – number of possible dislocation types

Burgers Vector

Edge Dislocations: 12
Screw Dislocations: 6

Dislocation Types: 2 x 18 = 36

dislocations of opposite sign needs to be distinguished

1,947,792 possibilities!

$$\begin{bmatrix} \kappa_{11} \\ \kappa_{21} \\ \kappa_{31} \\ \kappa_{12} \\ \kappa_{22} \\ \kappa_{32} \end{bmatrix} = \begin{bmatrix} \frac{1}{2} b_1^1 l_1^1 & \frac{1}{2} b_1^2 l_1^2 & \cdots & \frac{1}{2} b_1^{36} l_1^{36} \\ b_1^1 l_2^1 & b_1^2 l_2^2 & \cdots & b_1^{36} l_2^{36} \\ b_1^1 l_3^1 & b_1^2 l_3^2 & \cdots & b_1^{36} l_3^{36} \\ b_2^1 l_1^1 & b_2^2 l_1^2 & \cdots & b_2^{36} l_1^{36} \\ \frac{1}{2} b_2^1 l_2^1 & \frac{1}{2} b_2^2 l_2^2 & \cdots & \frac{1}{2} b_2^{36} l_2^{36} \\ b_2^1 l_3^1 & b_2^2 l_3^2 & \cdots & b_2^{36} l_3^{36} \end{bmatrix} \begin{bmatrix} \rho_G^1 \\ \rho_G^2 \\ \vdots \\ \vdots \\ \vdots \\ \rho_G^{36} \end{bmatrix}$$

6 known lattice curvatures (measured)

36 possible dislocation types

Not all dislocation types are equally energetically favourable.

$$w^t = \|\vec{b}^t\| \|\vec{l}^t\|$$

$$E_{screw} = (1 - \upsilon) E_{edge}$$

► With a set of 6 linear equations and 36 unknowns, a large number of possible solutions exists whereby a unique solution cannot be obtained. It is therefore necessary to constrain the solution using physically-based constraints.

Lower-bound GND Density

$$\rho_G = \sum_{t=1}^{36} \rho_G^t \approx \min \sum_{t=1}^{6} \rho_G^t$$

$$\sum_{t=1}^{6} w^t \rho_G^t = min$$

Simplex Optimisation Algorithm

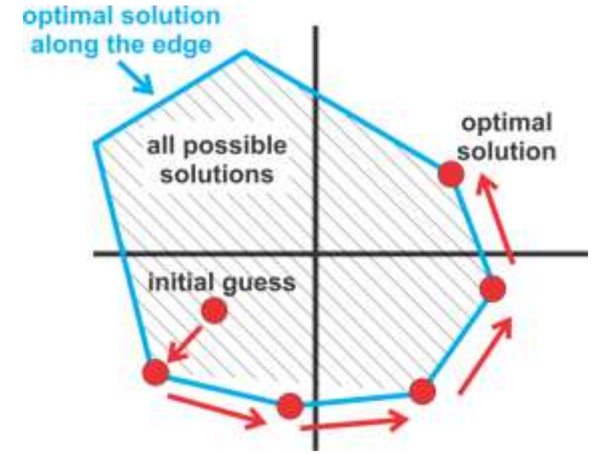

 | W. Pantleon, Scripta Materialia, 58, 2008, pp. 994-997.

ANSTO

GND Density

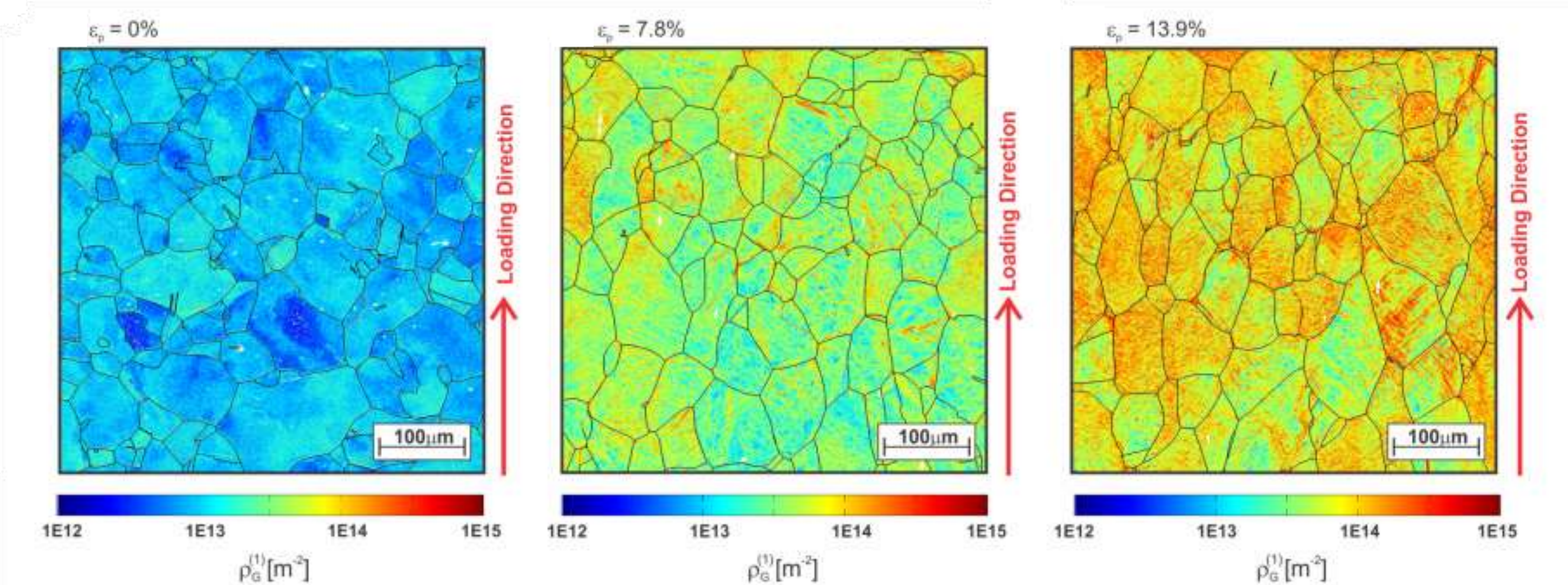

⇒ Density of geometrically-necessary dislocations (GND, ρ_G) maps calculated from the EBSD-measured Euler Angles (ϕ_1,Φ,ϕ_2) for specimens with 0% (as-received), 7.8% and 13.9% of imparted plastic strain.

⇒ Step size (h) = 200 nm
⇒ Magnification = 153x

⇒ Discrete measurements provide information on spatial distribution of GND across the microstructure.

⇒ GNDs arrange themselves into energetically favourable configurations forming geometrically-necessary boundaries (GNBs) subdividing grains into the sub-grains.

GND Spacing

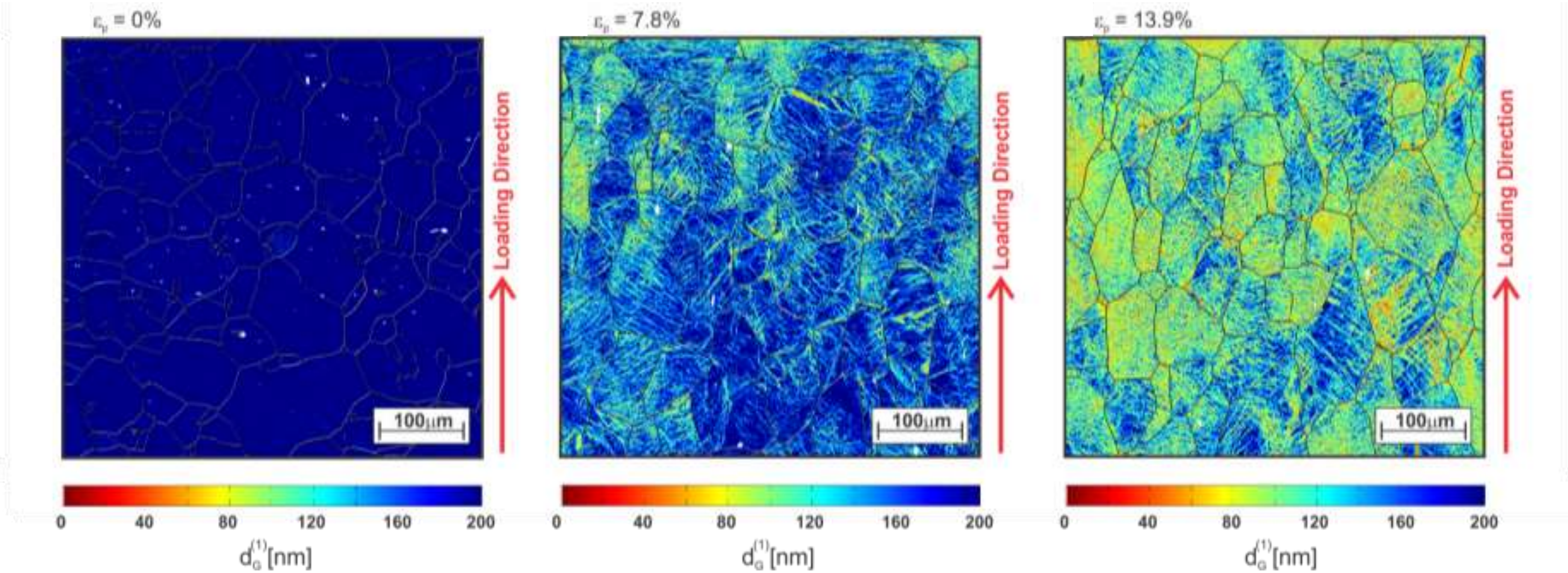

⇒ Spacing between geometrically-necessary dislocations (GND, d_G) recalculated from the GND density (ρ_G) for specimens with 0% (as-received), 7.8% and 13.9% of imparted plastic strain.

⇒ Non-uniform distribution of GNDs in the microstructure as GNDs arrange themselves into energetically favourable configurations subdividing grains into the sub-grains.

$$d_G = 1/\sqrt{\rho_G}$$

Dislocation spacing

GND Density

ANSTO

GND Density - High Resolution

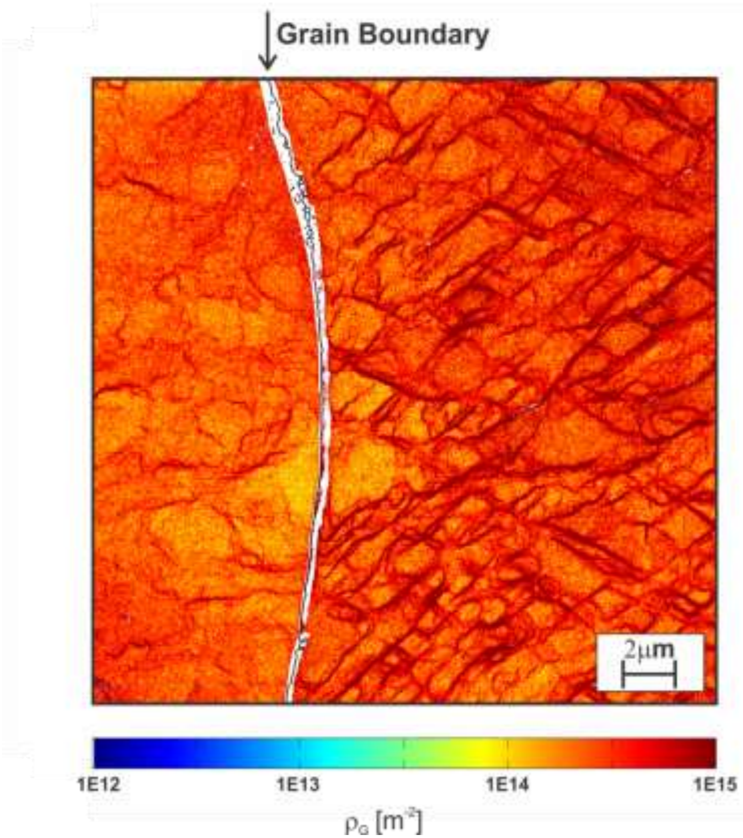

⇒ Density of geometrically-necessary dislocations (GND, ρ_G) calculated from the EBSD-measured Euler Angles (ϕ_1,Φ,ϕ_2).

⇒ Step size (h) = 20 nm
⇒ Magnification = 1000x

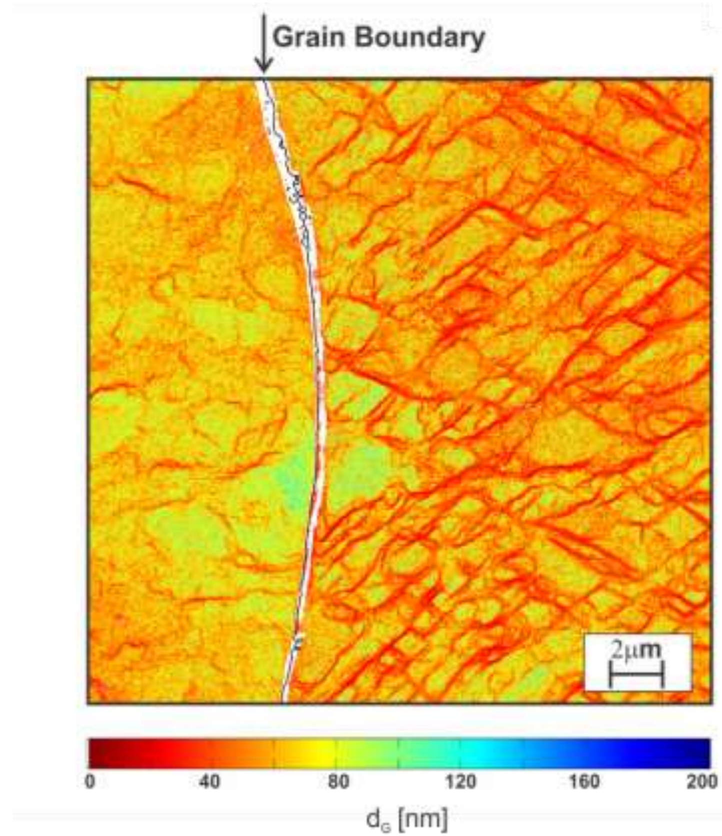

⇒ Spacing between geometrically-necessary dislocations (GND, d_G) recalculated from the GND density (ρ_G).

ANSTO

GND Density

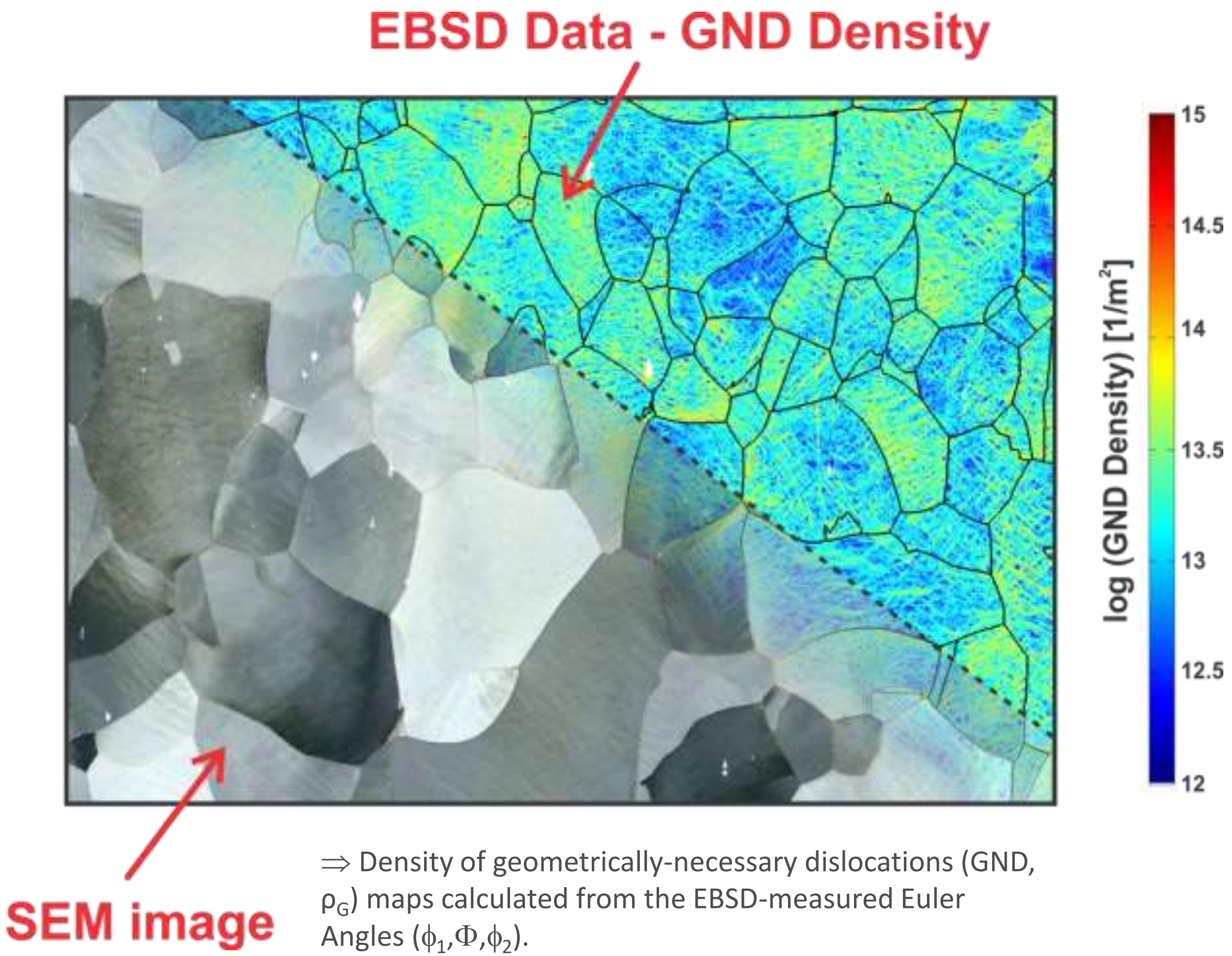

⇒ Density of geometrically-necessary dislocations (GND, ρ_G) maps calculated from the EBSD-measured Euler Angles (ϕ_1,Φ,ϕ_2).

Microstructure-Averaged GND Density

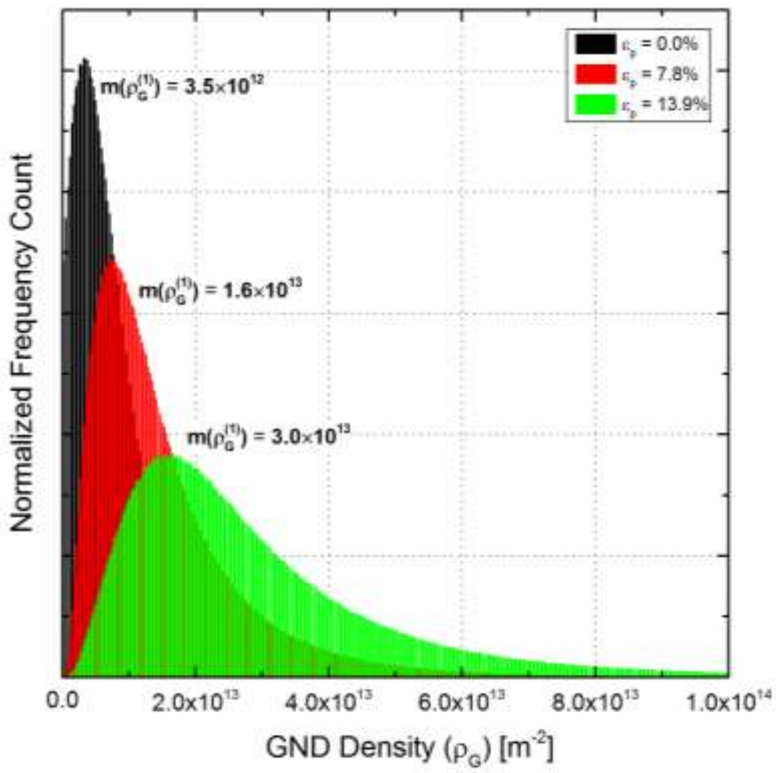

⇒ Distribution (histogram) of discrete GND density (ρ_G) measurements for specimen with 0% (as-received), 7.8% and 13.9% of imparted plastic strain (ε_p).

Log-Normal Distribution

$$f(\rho_G|\mu,\sigma) = \frac{1}{x\sigma\sqrt{2\pi}} exp\left(\frac{-(\ln(\rho_G)-\mu)^2}{2\sigma^2}\right)$$

MEAN of the log-normal distribution

Mean & Variance

$$m(\rho_G) = exp\left(\mu + \frac{\sigma^2}{2}\right)$$

$$v(\rho_G) = exp(2\mu + \sigma^2)(exp(\sigma^2)$$

VARIANCE of the log-normal distribution

⇒ The variance of the GND density distribution describes the heterogeneity of the GND distribution across variously oriented grains within the microstructure, the mean can be then taken as the microstructure-averaged (bulk) GND density.

Microstructure-Averaged GND Density

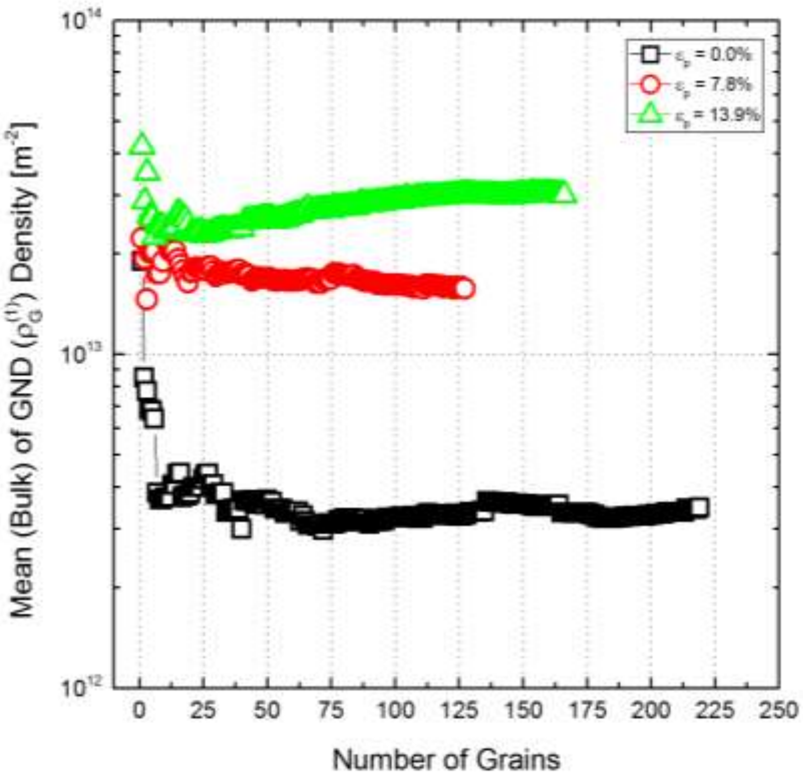

⇒ The development of the mean GND density as a function of number of analysed grains in GND density maps for specimen with 0% (as-received), 7.8% and 13.9% of imparted plastic strain (ε_p).

Log-Normal Distribution

$$f(\rho_G|\mu,\sigma) = \frac{1}{x\sigma\sqrt{2\pi}} exp\left(\frac{-(\ln(\rho_G)-\mu)^2}{2\sigma^2}\right)$$

Mean & Variance

MEAN of the log-normal distribution

$$m(\rho_G) = exp\left(\mu + \frac{\sigma^2}{2}\right)$$

$$v(\rho_G) = exp(2\mu+\sigma^2)(exp(\sigma^2)$$

VARIANCE of the log-normal distribution

⇒ Due to the increase in heterogeneity of GND distribution with imparted plastic strain, a larger number of grains is required to reach solution convergence.

Microstructure-Averaged GND Density

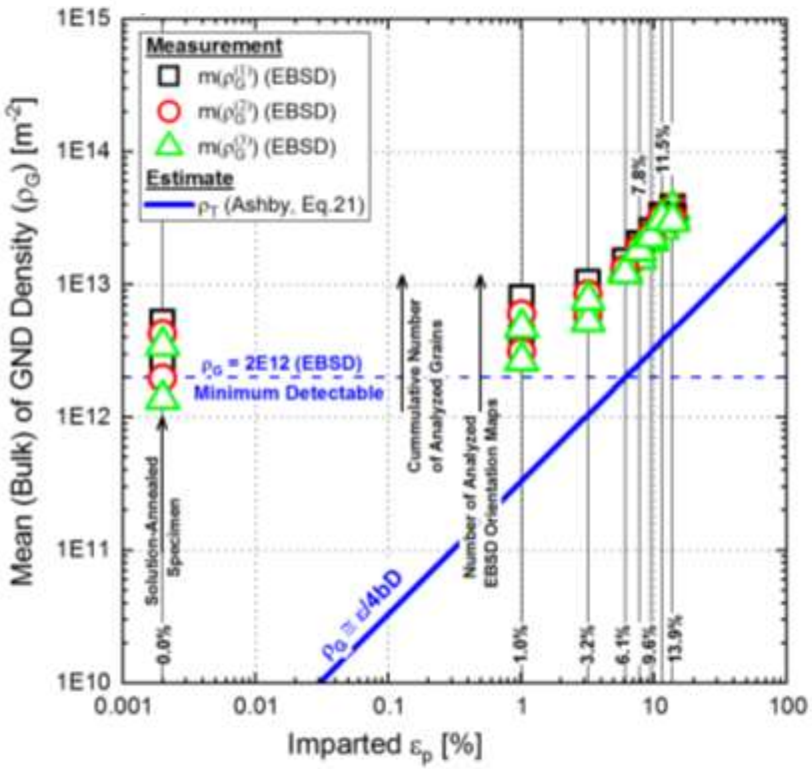

⇒ The development of the **mean** GND density distribution as a function of imparted plastic strain (ε_p) for all tested specimens.

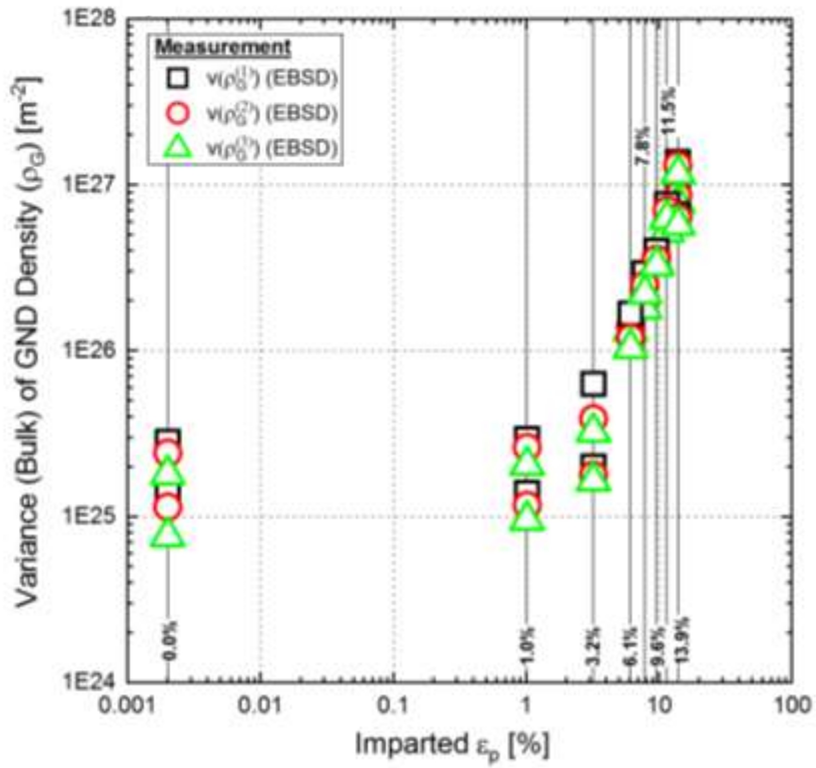

⇒ The development of the **variance** of GND density distribution as a function of imparted plastic strain (ε_p) for all tested specimens.

GND Types in Solution

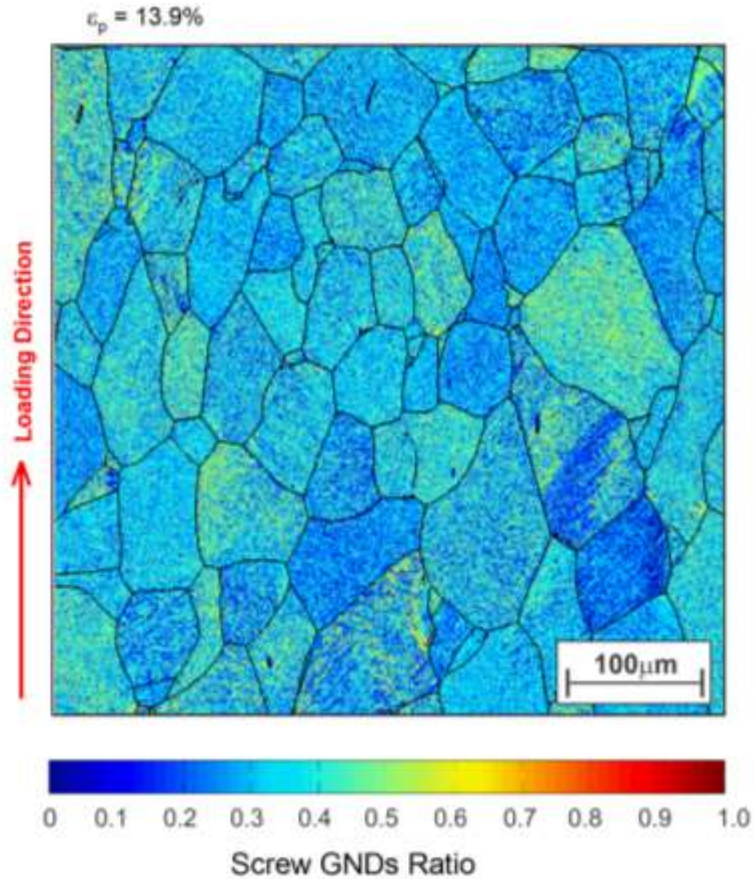

⇒ Map showing the ratio of screw dislocations to the total number of dislocations in the solution (6) for the specimen with 13.9% imparted plastic strain.

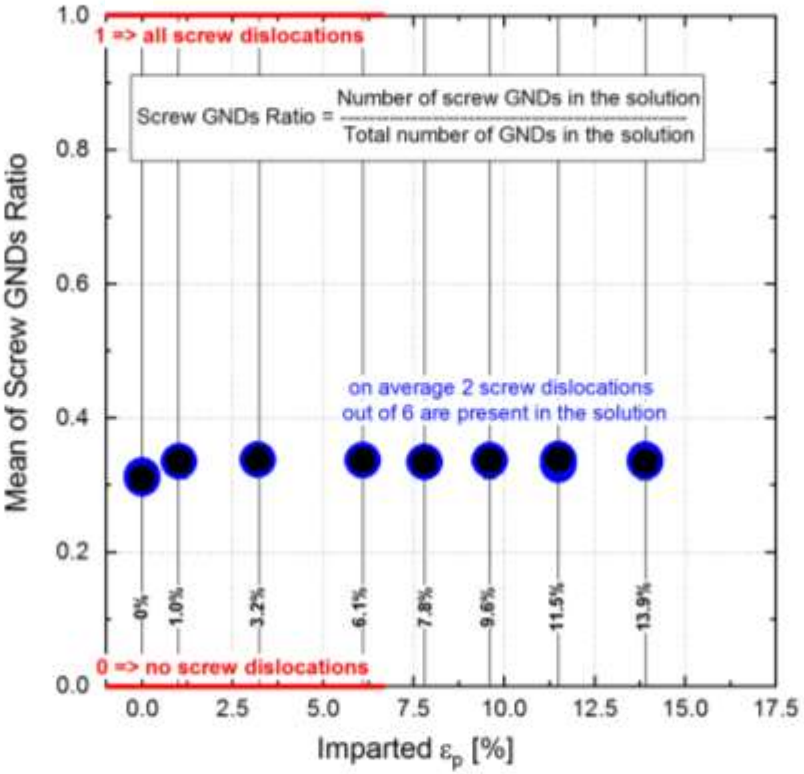

⇒ Screw dislocation ratio as a function of imparted plastic strain for all tested specimens.

⇒ The uniqueness of the solution is not guaranteed.
⇒ Only pure edge and pure screw dislocations have been considered in the calculation.

ANSTO

HRSD Measurements

HRSD Set-Up

- Detector: 2048 × 2048 pixels
- Pixel Size: 200 × 200 µm
- Distance: 1873 mm

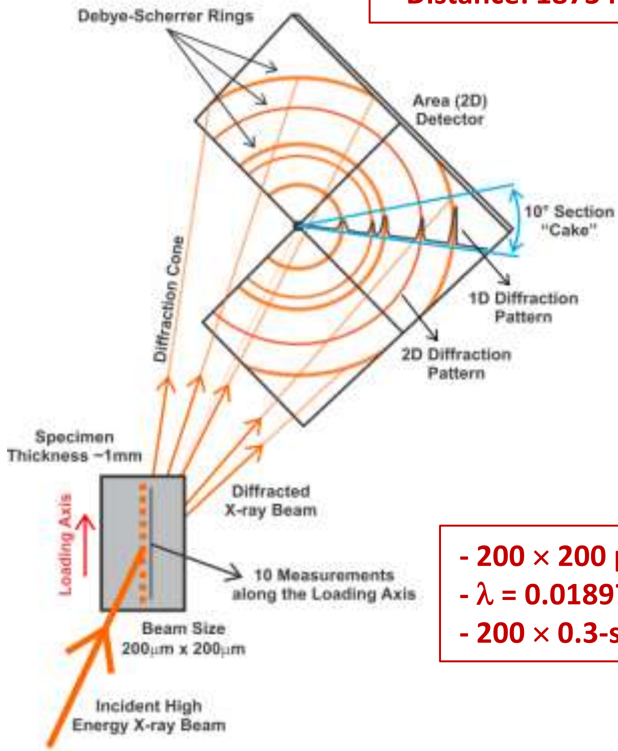

- 200 × 200 µm
- λ = 0.018972 nm
- 200 × 0.3-s intervals

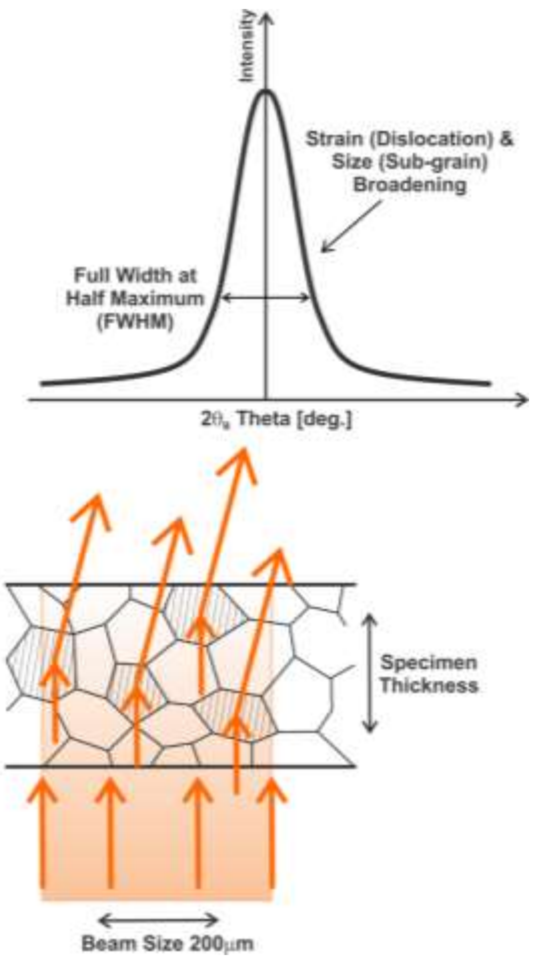

⇒ High-resolution synchrotron diffraction (HRSD) set-up at 1-ID high-energy beamline at the Advanced Photon Source (APS), Argonne National Laboratory (ANL).

Diffraction Peak Broadening

⇒ The total diffraction peak shape (which includes peak broadening) I_{TOTAL} of a is the convolution of the shape contribution caused by the size of coherently scattering domains (sub-grains) I_{SIZE} and the contribution caused by strain fields of present dislocations I_{STRAIN}.

⇒ Convolution is defined as the invers Fourier transform of the product of the individual Fourier transform of the components.

$$I_{TOTAL} = I_{SIZE} * I_{STRAIN} = \mathcal{F}^{-1}\left(A^{Size} A^{Strain}\right)$$

$$A^{Size} = \mathcal{F}(I_{SIZE}) \quad A^{Strain} = \mathcal{F}(I_{STRAIN})$$

Size (sub-grain) contribution to the peak shape.

Strain (dislocation) contribution to the peak shape.

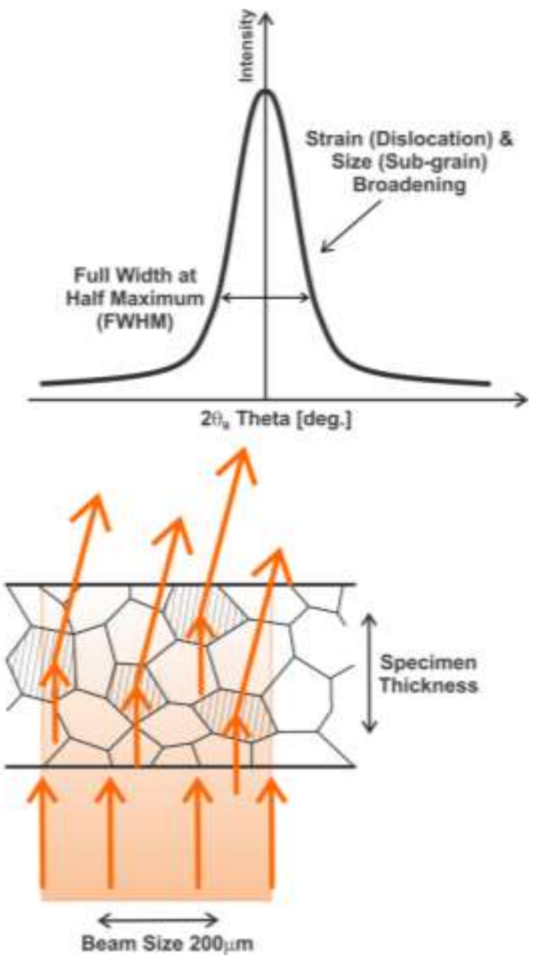

 T. Ungar et al., J. Appl. Cryst. 34, 2001, pp. 298-310.

Diffraction Peak Broadening

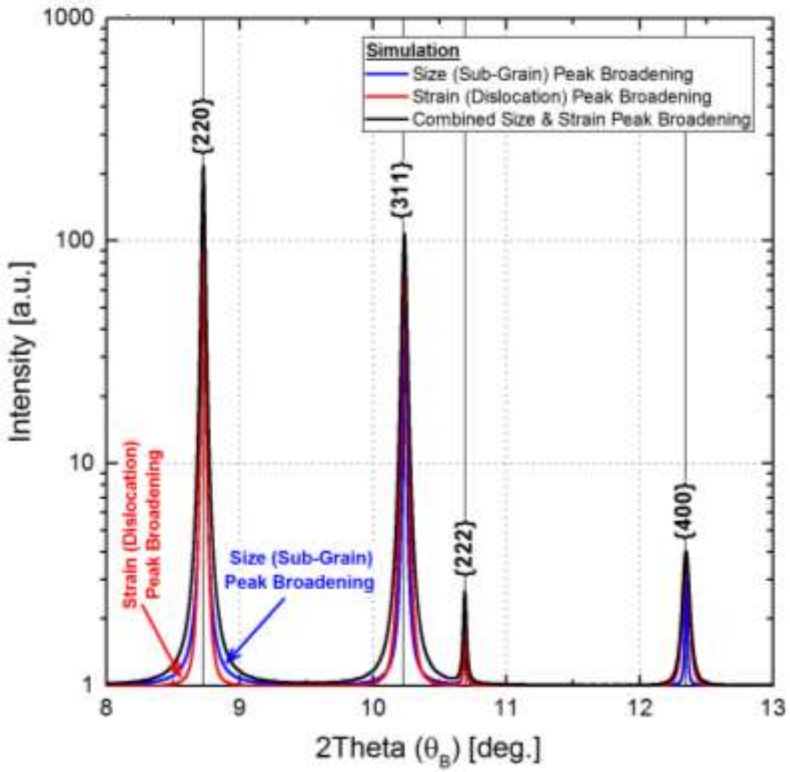

Williamson-Hall Plot

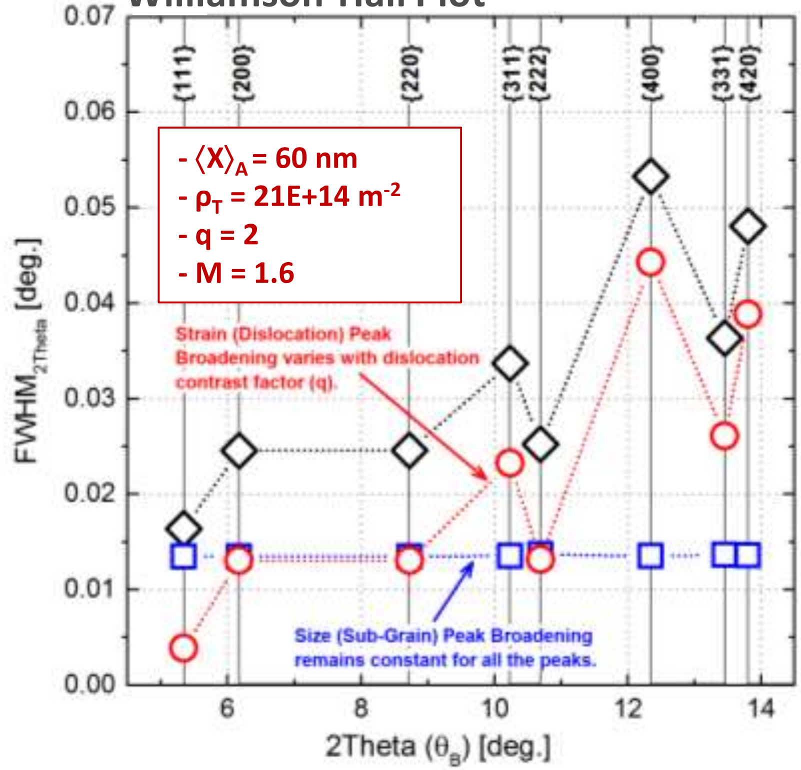

⇒ The broadening due to the size of the coherently diffracting domains (sub-grains) is the same for all hkl diffraction peaks, while the broadening component due to the strain field of present dislocations varies between diffraction peaks. This variation in the strain (dislocation) broadening is not monotonous due to the anisotropic behaviour described by the dislocation contrast factors.

T. Ungar et al., J. Appl. Cryst. 34, 2001, pp. 298-310.

Diffraction Peak Broadening

⇒ 2D diffraction pattern (Debye-Scherrer rings) of specimen with 13.9% of imparted plastic strain.

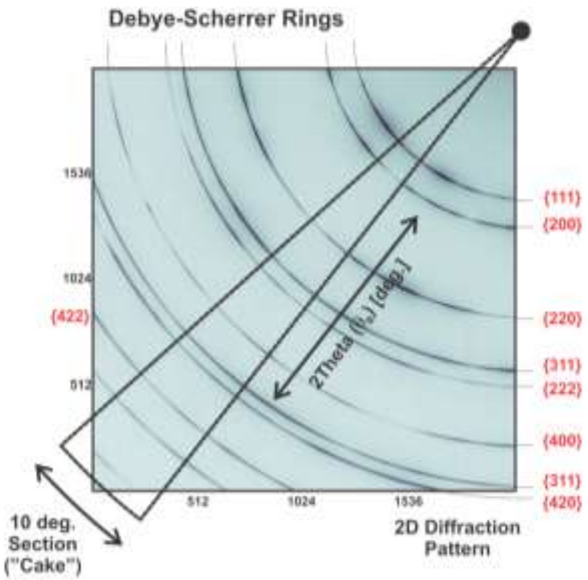

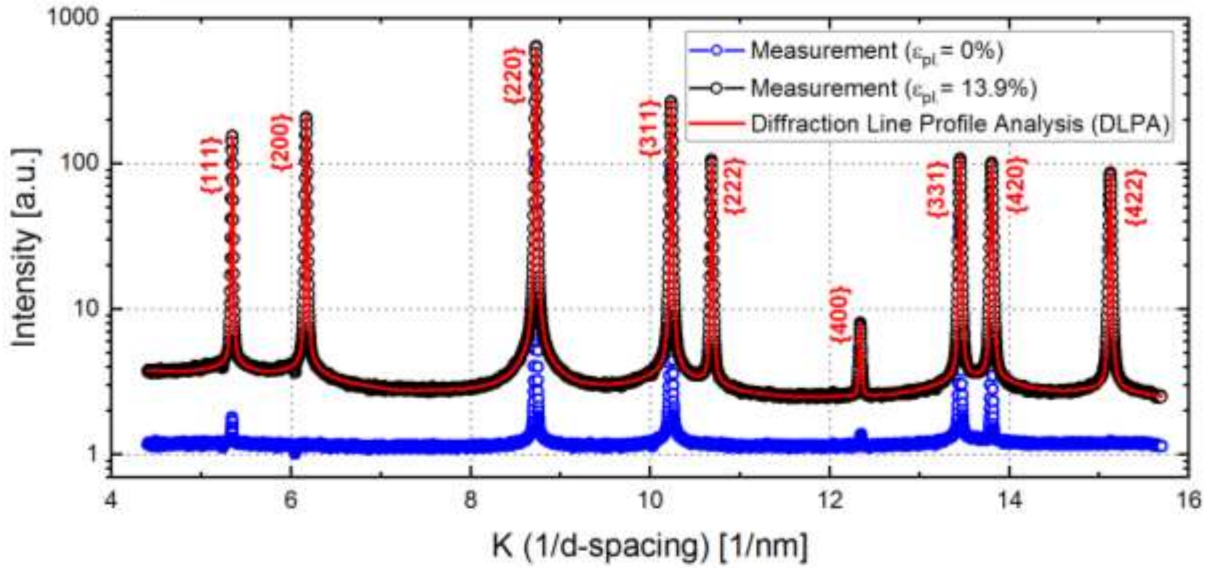

⇒ Comparison of full diffraction patterns for specimens with 0% (as-received) and 13.9% of imparted plastic strain. The different behavior of size (sub-grain) and strain (dislocation) peak broadening can be resolved if many peaks are available.

⇒ The diffraction peak broadening was analysed using the eCMWP (extended Convolutional Multiple Whole Profile) LPA software

ANSTO

Total Dislocation Density & Sub-Grain Size

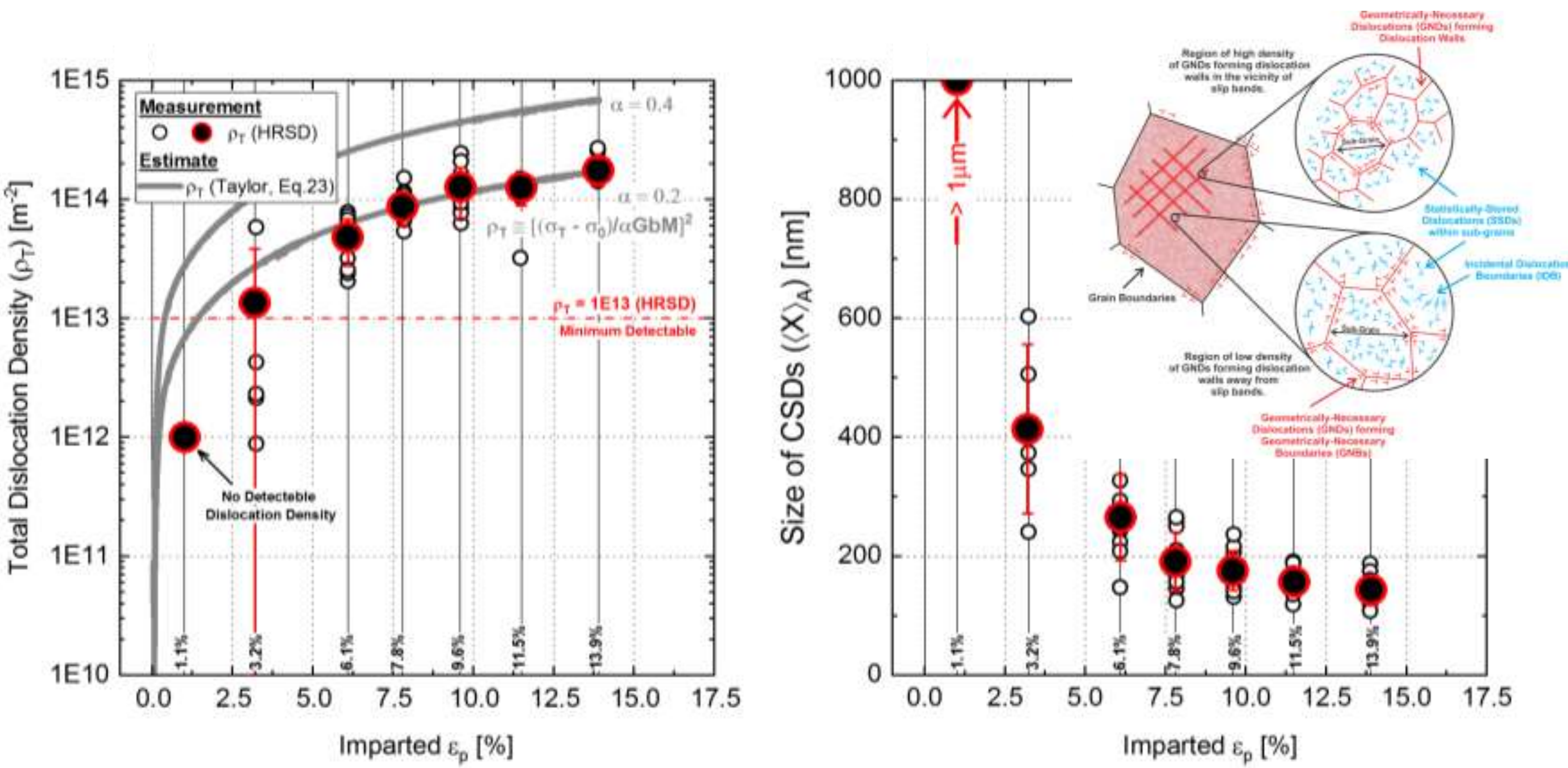

⇒ Total dislocation density (ρ_T) and size of the coherently scattering domains (SCDs) obtained by line profile analysis (LPA) of HRSD patterns as a function of imparted plastic strain (ε_p) - open symbols represents individual measurements along the sample loading axis, and solid symbol represents the mean values.

ANSTO

EBSD + HRSD Measurements

EBSD- & HRSD- Measured Dislocation Density

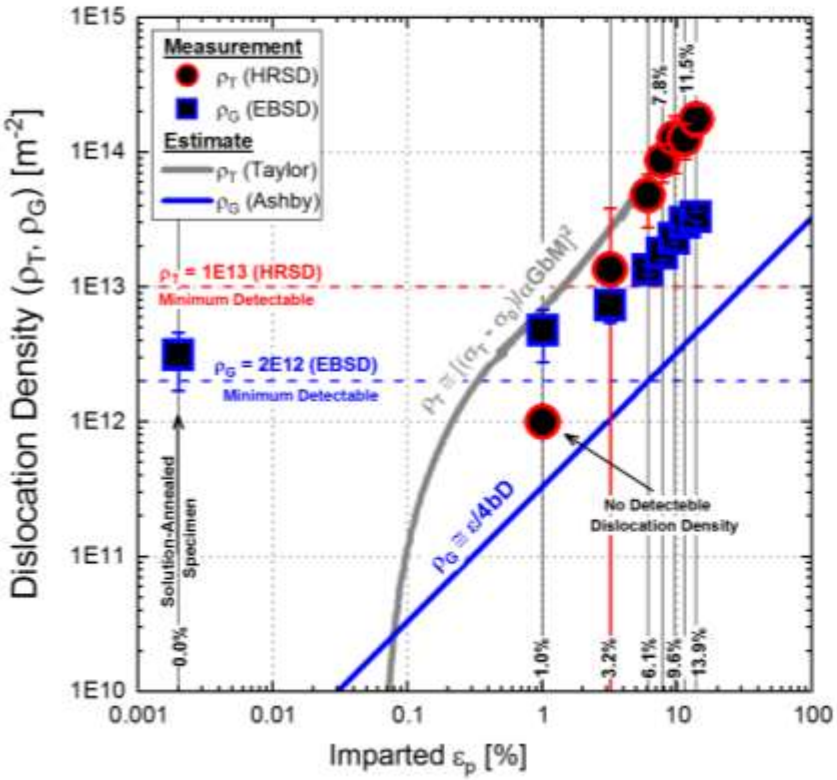

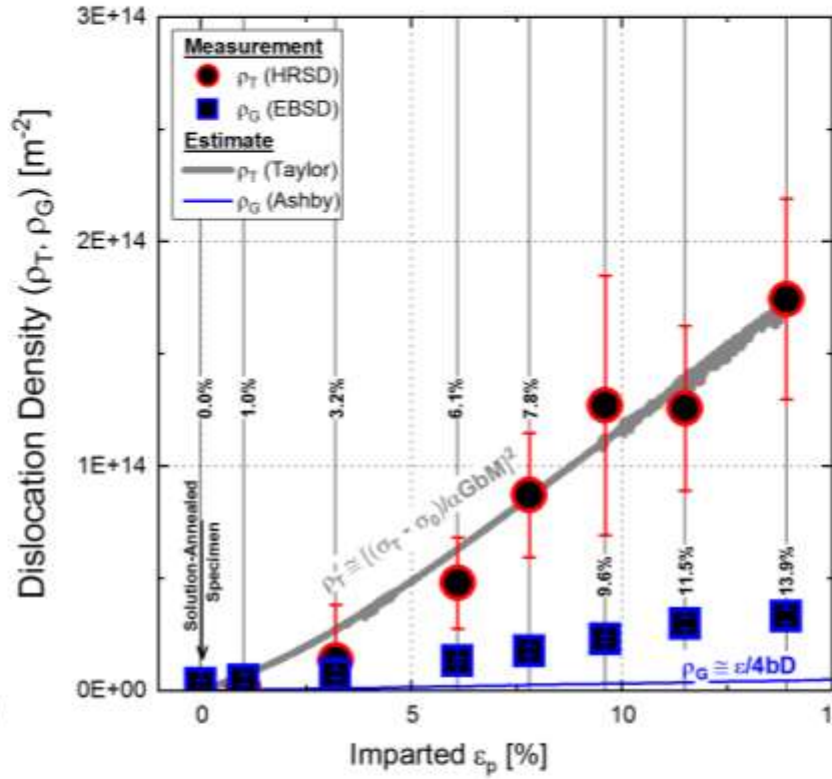

⇒ Comparison of the HRND-measured total dislocation density (ρ_T) and the EBSD-measured density of GNDs (ρ_G), together with expected dislocation densities calculated using the modified Taylor's model, and single-slip Ashby's model.

⇒ Both GNDs and SSDs contribute to the work-hardening of the material.
⇒ SSDs represent more than 80% of all the present dislocations.

ANSTO

GND Density & Size of CSDs

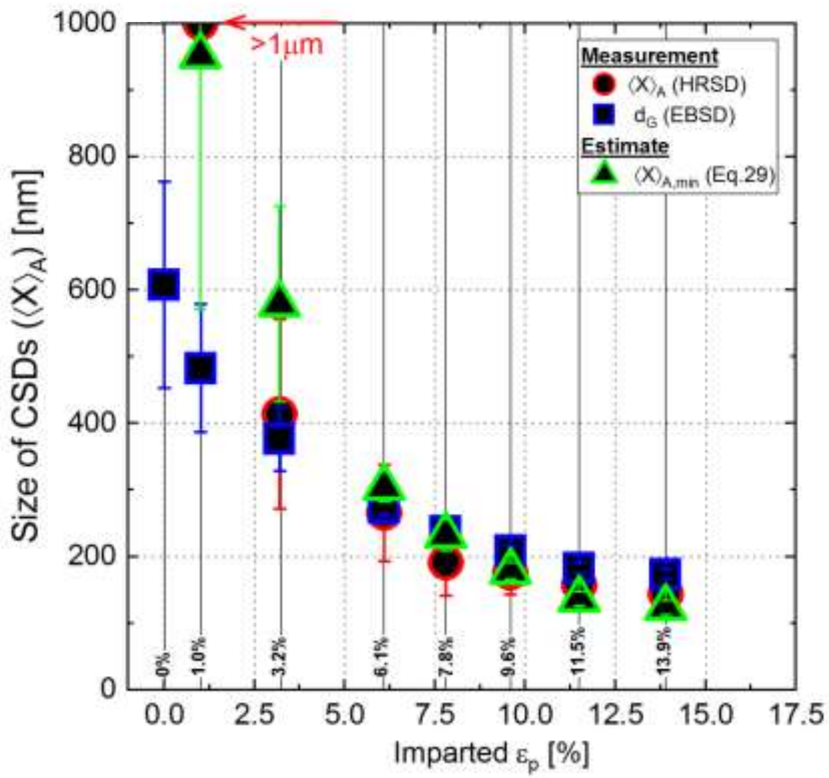

⇒ Comparison of the HRSD-measured size of CSDs (red circles) with EBSD-measured spacing of GNDs (d_G) (blue squares), and the estimated minimum size of CSDs (green triangles) from EBSD-measured density of GNDs (ρ_G).

Size of SSDs from ρ_G

$$\langle X\rangle_A \geq \langle X\rangle_{A,min} = \sqrt{\frac{2}{3}\frac{1}{\Delta x \rho_G}} = \sqrt{\frac{2}{3}\frac{d_G^2}{\Delta x}}$$

GNDs spacing; EBSD step size; GNDs density

ρ_G from $\langle X\rangle_A$

$$\rho_G \geq \sqrt{\frac{2}{3}\frac{1}{\Delta x \langle X\rangle_A}}$$

EBSD step size; Size of SSDs

⇒ This defines the connection between EBSD-measured ρ_G and HRSD-measured $\langle X\rangle_A$ one can then estimate ρ_G from $\langle X\rangle_A$.

Conclusions

- ⇒ EBSD measures the lower-bound ρ_G, while HRSD measures ρ_T.
- ⇒ The minimum detected ρ_T measured by HRSD is about **1E13 m^{-2}**, while the minimum ρ_G measured by EBSD is about **2E12 m^{-2}**.
- ⇒ EBSD is more sensitivity to the small amount of plastic deformation in the material, while HRSD gets more accurate with higher amount of plastic deformation.
- ⇒ There is a connection between EBSD-measured ρ_G and HRSD-measured size of CSDs ($\langle X \rangle_A$).
- ⇒ **EBSD** = Density of GNDs (ρ_G), **+ estimate the minimum Size of CSDs**
- ⇒ **HRSD** = Total Dislocation Density (ρ_T), size of CSDs ($\langle X \rangle_A$), **+ estimate of minimum density of GNDs (ρ_G)**

GNDs spacing

$$\langle X \rangle_A \geq \langle X \rangle_{A,min} = \sqrt{\frac{2}{3}\frac{1}{\Delta x \rho_G}} = \sqrt{\frac{2}{3}\frac{d_G^2}{\Delta x}}$$

EBSD step size

GNDs density

Australian Government | ANSTO

Thank you for your time and interest in this work. We hope you will find it useful.

Developed Matlab code for calculation of GNDs is available as a supplementary material with out Acta Materialia paper.